Applied and
Computational
Mechanics

Research and evaluation of the impact of air: Cooling models on the operating temperature of lithium-ion batteries

P. M. Hieu[a], D. V. Tuan[a,b,*], D. D. Thanh[a,c], N. T. Kien[a], N. D. Trong[a]

[a]*School of Mechanical and Automotive Engineering, Hanoi University of Industry, Hanoi, Vietnam*

[b]*Department of Mechanical and Computer-Aided Engineering, National Formosa University, Huwei Township, Yunlin County, Taiwan*

[c]*Institute of Engineering and Technology, Vinh University, Nghean, Vietnam*

Abstract

In this study, a Panasonic 18650 lithium-ion battery module consisting of 24 cells with multiple vents was studied and the design was optimized through numerical simulation. Compared to previous studies showing that the cooling model layout using 1 inlet and 1 outlet was improved, the cooling model with multiple vents improved the temperature difference and the maximum temperature in the cells. Specifically, the effects of multiple directions and the number of inlet/outlet cooling air were analyzed in the study, and finally the appropriate inlet velocity was discovered to be applied on the proposed model. The results showed that the arrangement of 2 inlets air holes at the center of the two ends of the battery module and 1 outlet hole at the center of the bottom surface produced the best cooling effect compared to the first model and other models. The maximum temperature (T_{max}) and maximum temperature difference (ΔT_{max}) were reduced by 312.62 K (14 %) and 6.74 K (88 %), respectively compared to the first model. Furthermore, with the 2 inlets – 1 outlet model being the optimal cooling model for the selected model, consideration of the velocity input value to bring the model to operate in the appropriate temperature range was then carried out. The results showed that with the battery cell operating at a discharge current of 3 C, velocity higher than $2 \, \mathrm{m \, s^{-1}}$ was sufficient for the battery module to operate at the maximum temperature (T_{max}) and maximum temperature difference (ΔT_{max}) of 306.69 K and 4.84 K, respectively without consuming much fan power.
© 2025 University of West Bohemia in Pilsen.

Keywords: air cooling, computational fluid dynamics, battery thermal management, multiple air vents

1. Introduction

Nowadays, developed countries often require a large amount of fossil fuel for industrial production [1]. This leads to a serious depletion of natural resources and negative environmental impacts [11]. At the same time, industrial development has resulted in a dramatic increase in transportation vehicles, which is a major contributor to the emission of pollutants from automobiles into the environment [7]. Although there have been studies on more environmentally friendly fuels such as bioethanol [22] and biodiesel [44], the overarching goal is to replace fossil fuels, which have high emission rates, with alternative energy sources [45]. Nevertheless, these alternatives have not yet fully addressed the major drawbacks associated with the use of fossil fuels. Therefore, renewable resources such as solar energy, wind energy, tidal energy, etc., are being focused on as potential alternatives to non-renewable fuels [8]. However, a drawback of harvesting energy from these sources is the uneven energy production due to their heavy dependence on weather conditions [6]. Consequently, the use of a battery system for energy storage

is an excellent method to maintain and store energy by converting it into chemical reactions within the battery, which can be reverted into electrical energy when needed [32].

In the automotive industry, the transition from traditional internal combustion engine vehicles to electric vehicles is becoming increasingly common in many countries around the world. Some leading nations in the electric vehicle transition include the United States, China, and various European countries [4, 9, 42]. Researchers estimate that in the next 10–20 years, 20–35% of all vehicles produced will be electric [3, 21, 38]. Lithium batteries are currently considered to offer the best performance and are widely used by electric vehicle manufacturers across various types of vehicles, such as fully electric vehicles, self-charging hybrids, and plug-in hybrids [32]. The widespread use of lithium batteries in electric vehicles is understandable because they provide longer driving ranges due to their high energy density. Moreover, they are lightweight, have high specific power, no memory effect, and a long cycle life [23]. However, the performance of lithium batteries is significantly affected by temperature. According to previous studies, the ideal operating temperature range for lithium battery modules is from 293 to 313 K, with a temperature difference of no more than 5 K between cells [5, 28]. Excessively high or low temperatures can lead to abnormal battery operation, which in turn poses risks of fire or explosion. Low temperatures reduce battery performance due to increased internal resistance, while high temperatures shorten battery lifespan as chemical reactions become more intense and accelerate degradation [17]. For this reason, battery modules require a thermal management system to effectively and reliably maintain and control temperature differences within the battery module.

Over decades of research and development, many thermal management technologies for battery modules have been introduced, including liquid cooling systems [25, 29], phase change material (PCM) cooling systems [10, 19], air cooling systems [18, 36], and hybrid systems that combine different methods [16, 40]. Among these, liquid cooling provides excellent performance by maintaining uniform temperature and effectively dissipating heat. However, this method requires high costs due to installation components such as pumps, piping, and sensors, which significantly increase the vehicle's weight [34]. Moreover, the system requires regular maintenance due to potential leakage risks that could endanger the electrical system. In contrast, PCM-based cooling systems face limitations in cooling capacity due to material properties. Additionally, the cooling ability is difficult to restore because PCM requires time to solidify again to function properly [31]. Recent efforts in battery thermal management have moved beyond conventional cooling systems. A growing body of research is focused on developing advanced solutions, including the design of innovative heat sinks integrated with nano-enhanced PCM [27], optimizing the heat transfer performance of indirect liquid-cooled modules through circuitous minichannel designs [31], and notably, the application of AI and digital twin technologies for intelligent battery management and lifecycle optimization [15, 20]. These advancements underscore the multidimensional direction of the field in addressing thermal challenges. Therefore, air cooling systems—with their advantages of simple structure, low production and maintenance costs, and high reliability—are still being actively researched to improve their cooling performance [41]. The reduction of temperature differences between battery cells using axial ventilation—by designing secondary air inlets on various faces of the battery module—was proposed by Shahid et al. in [30]. Li et al. [14] presented an air-cooling model for a battery module with an inlet at one end and an outlet on the opposite side, combining computational fluid dynamics (CFD) simulations with experimental validation. In [43], Zhou et al. mitigated temperature differences by incorporating cylindrical air distribution channels into the battery module and analyzed the effects of hole parameters, inlet pressure, and discharge

speed on cooling performance using a combined numerical modeling approach. Previous studies focused on structural optimization. Specifically, Koorata and Chandrasekaran [13], through numerical analysis of an air-cooled thermal management system integrated with thermal interface material, demonstrated that shifting the inlet/outlet boundary location to a central position enhances temperature uniformity, reducing the temperature difference from $4.4\,°\mathrm{C}$ to $3.1\,°\mathrm{C}$ at a discharge rate. However, these works, including [12, 13, 35], primarily discussed the influence of ventilation hole positioning but were limited to analyzing vent configurations with only a single inlet and a single outlet. In [33], Turaka et al. utilized CFD simulation for in-depth thermal analysis, confirming that liquid cooling significantly outperforms air cooling in terms of thermal performance, reducing the maximum temperature by up to 3.3 K during 2 C discharge, thereby underscoring the imperative for optimizing air-cooling systems to overcome these inherent limitations. In general, previous studies have attempted to reduce temperature variation within battery modules by altering the location of vents, airflow direction, and hole parameters. However, there has not yet been a comprehensive study combining all three factors; instead, existing research has addressed them individually.

Therefore, in this study, the aim is to provide evaluation surveys in changing the number, location and size of vent holes to the proposed lithium module model, including 24 cells and the module housing. CFD software ANSYS Fluent is used as a reliable simulation tool to evaluate the thermal performance in each case. The values of the maximum module temperature ($T_{\max}$) and the maximum temperature difference ($\Delta T_{\max}$) will be discussed comprehensively to evaluate and obtain the model with the best cooling performance.

2. Model and solution approach

2.1. Numerical model design

The proposed battery module is air-cooled using forced convection and consists of 24 battery cells arranged in a $4{\times}6$ configuration, enclosed within an outer casing. The model was modeled using SolidWorks software and is shown in Fig. 1. Cooling vents are placed at the center of faces A and C, following the optimized model published in the study by Koorata and Chandrasekaran [13]. The basic dimensions of the battery cells are: height of 65 mm, diameter of 19 mm, with a 1 mm spacing between adjacent cells, and a 20 mm gap from the top of the cells to the casing. The dimensions of the outer casing are 140 mm in length, 100 mm in height, and
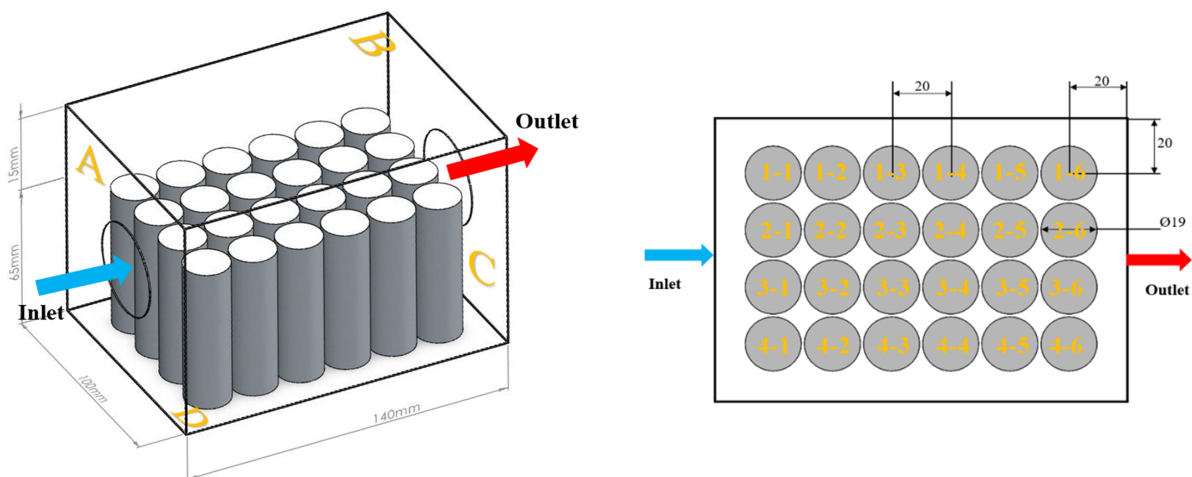

Fig. 1. Model of the air-cooled battery module

Table 1. Location designed ventilation holes

Configuration	Inlet location(s)	Outlet location(s)
1 inlet – 1 outlet	A	C
1 inlet – 2 outlets	A	B and C
1 inlet – 3 outlets	A	B, C and D
2 inlets – 1 outlet	A and B	C
2 inlets – 2 outlets	A and B	C and D
3 inlets – 1 outlet	A, B and C	D

80 mm in width. Each cell is labeled according to a row-column format, numbered from left to right (following the direction of airflow) and from top to bottom. The ventilation holes are arranged at the center of faces A, B, C, and D to allow the cooling air to circulate symmetrically and efficiently. The heat generated during battery operation is removed by the airflow passing through the module. CFD software, ANSYS Fluent, is used in this study to perform the simulations.

The test cases involving different numbers and placements of ventilation holes are designed to maintain a constant total airflow rate for both inlet and outlet in all scenarios. Since the study considers only the four faces A, B, C, and D, the maximum number of inlet or outlet holes is limited to 3. Therefore, the diameter of each hole in different scenarios is as follows: 1 inlet/outlet hole: 40 mm, 2 inlets/outlets holes: 28 mm, and 3 inlets/outlets holes: 20 mm. The specific configurations for the placement of inlet and outlet ventilation holes, corresponding to the number of holes ranging from 1 to 3, are shown in Table 1.

2.2. Boundary conditions and grid independence evaluation

The inlet air velocity in this study is set at $1 \, \text{m s}^{-1}$, corresponding to an airflow rate of $1.25 \times 10^{-3} \, \text{m}^3 \, \text{s}^{-1}$ for the case with a single inlet. When the number of inlets increases, the total airflow rate is evenly distributed among each inlet. The inlet air temperature is set to 298 K, corresponding to ambient temperature, and the pressure is set to atmospheric pressure. A velocity inlet condition and a pressure outlet condition are applied. The module casing is set with a no-slip boundary condition, and the relative pressure at the outlet is set to zero. Since battery modules are usually installed in compact and confined spaces, adiabatic boundary conditions are applied to the outer surfaces of the module. Additionally, thermal radiation emitted by the cells is neglected in this study. Table 2 presents the material properties used in the simulation. The material properties used in the simulations were primarily derived from previous studies, including [26, 39]. These data were supplemented with experimental information obtained from the ANSYS material database, as summarized in Table 2.

To ensure the accuracy of the simulation, a mesh independence test was conducted. The numerical simulations were performed based on the finite volume method (FVM), implemented in the ANSYS Fluent environment. The maximum temperature variation of the model was eval-

Table 2. Material parameters used in simulation

Material	$c \, [\text{J kg}^{-1} \, \text{K}^{-1}]$	$\varrho \, [\text{kg m}^{-3}]$	$k \, [\text{W m}^{-1} \, \text{K}^{-1}]$	$\mu \, [\text{Pa s}]$
Battery	1 200	2 500	4	–
Cooling air	1 005	1.204	0.0267	1.5×10^{-5}

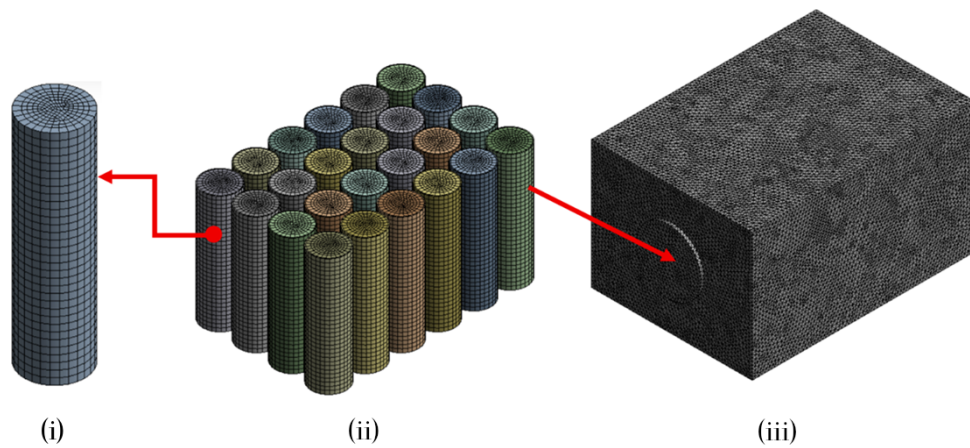(i)   (ii)   (iii)

Fig. 2. Meshing system diagram for battery module: (i) straight view of a single 18650 cell, (ii) straight view of the entire cell in the module, (iii) straight view of the entire module

Table 3. Lithium-ion battery specifications

Length [mm]	Diameter [mm]	Minimum voltage [V]	Normal voltage [V]	Maximum voltage [V]	Capacity [mAh]
65	18	2.5	3.6	4.2	3 000

uated under five different mesh densities, as presented in Figs. 2–3. The results show that as the total number of mesh elements increased from 707 296 to 4 200 244, the maximum temperature within the battery module changed from 328.8851 K to 328.8084 K, respectively. With a minimal difference of only 0.734 K between these two mesh densities, as shown in Fig. 3, the mesh containing 707 296 elements, as illustrated in Fig. 2, was considered sufficient for accurate prediction and was therefore adopted for the present study.

2.3. Physical model of the battery module

The commercial Panasonic 18650 lithium – ion battery (LIB) model is selected for this study. The detailed specifications of the battery are presented in Table 3.

An air-cooled lithium battery pack consists of two main components: the lithium-ion battery
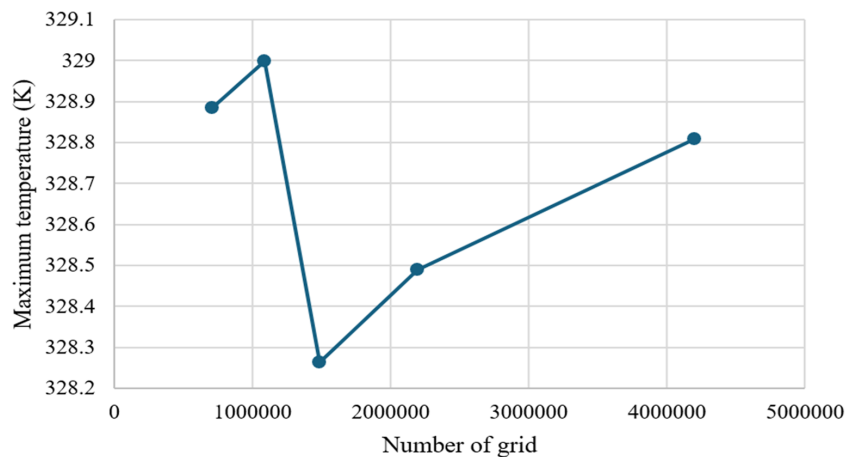

Fig. 3. Mesh independence test

(LIB) cells and the cooling gas. The governing equations for these two domains are as follows:

A) Heat generation from the battery

The heat generated within the battery cells is expressed by the energy balance equation [37]

$$\dot{Q} = (V - V_{OCV})\,I + IT\frac{\mathrm{d}V_{OCV}}{\mathrm{d}T}, \tag{1}$$

where V is the cell voltage, V_{OCV} represents the open-circuit voltage, I is the operating current, and T is the cell temperature.

In this study, all simulations are performed at a discharge rate of $3\,\mathrm{C}$ (C-rate refers to the charge or discharge current normalized to the nominal capacity of the battery where $1\,\mathrm{C}$ means the battery is fully charged or discharged in one hour), and effects related to battery aging, variations in internal resistance, and nonuniform heat generation among cells are not considered. Furthermore, each 18650 cell was modeled as a homogeneous thermal body without explicitly analyzing the tab region. The volumetric heat generation rate inside LIB is taken as $48{,}750\,\mathrm{W\,m^{-3}}$ based on the heat generation formula within the battery tab, expressed as follows [2]:

$$Q_t = RI^2, \tag{2}$$

where R is the internal resistance of the lithium battery. The value of R is taken as $R = 10\,\mathrm{m\Omega}$.

B) Governing equations for the cooling airflow

With the inlet velocity and airflow rate conditions for the cooling air as presented in Section 2.2, when the number of inlet holes increases from 1 to 3, the Reynolds number decreases from 7 384 to 3 785. The Reynolds number at the inlet is defined as follows:

$$\mathrm{Re} = \frac{\varrho\,vD}{\mu}, \tag{3}$$

where ϱ is the density of air, v is the velocity of air, D is the characteristic diameter of the inlet hole, and μ is the dynamic viscosity of air. Since the Reynolds number is greater than $2\,300$, turbulent flow regime is applied for the air-cooling system of the lithium battery. The governing equations for turbulent flow are presented as follows: Considering a turbulent, single-phase, incompressible fluid, the conservation equations of momentum, energy, and mass are [24]:

$$\varrho_f\frac{\partial\overline{\boldsymbol{v}}}{\partial t} + \varrho_f\left(\overline{\boldsymbol{v}}\cdot\nabla\right)\overline{\boldsymbol{v}} = -\nabla\overline{p} + \left[\nabla\left(\mu\nabla\overline{\boldsymbol{v}}\right) - \varphi\right], \tag{4}$$

$$\varrho_f\frac{\partial T_f}{\partial t} + \varrho_f\nabla\cdot\left(\overline{\boldsymbol{v}}\,T_f\right) = \nabla\left[\left(\frac{\mu}{\mathrm{Pr}} + \frac{\mu_t}{\mathrm{Pr}_t}\right)\nabla T_f\right], \tag{5}$$

$$\nabla\cdot\overline{\boldsymbol{v}} = 0, \tag{6}$$

where p is the pressure, φ represents the Reynolds stresses, T is the gas temperature, Pr is the Prandtl number, and Pr_t denotes the turbulent Prandtl number.

The characteristics of the turbulent flow are simulated in ANSYS Fluent software using the standard $k\text{–}\varepsilon$ turbulence model.

3. Results and simulations

During continuous discharge at a $3\,\mathrm{C}$ rate, the battery temperature continuously rises due to electrochemical reactions and heat exchange among the cells within the module. This heat

is removed by the airflow passing through the ventilation holes. The objective of this study is to maintain all cells in the module operating within the optimal temperature range T_{max} of 283–313 K and the temperature difference ΔT_{max} between cells is not more than 5 K. These parameters will be sought through the simulations performed in software ANSYS Fluent. First, the study presents the results of the cooling model using 1 inlet.

3.1. Thermal performance of the 1 inlet – N outlet(s) configuration

A) 1 inlet – 1 outlet model
To verify the accuracy of the proposed model in this study, the 1 inlet – 1 outlet model was constructed based on the battery module structure published by Koorata and Chandrasekaran in [13].

The results in Fig. 4 show a significant temperature distribution difference among the battery cells in the 1 inlet – 1 outlet module. It is easy to observe that the cells located at positions (1–1), (2–1), (3–1), and (4–1), which are near the inlet, are effectively cooled. However, the cooling efficiency decreases significantly for the columns of cells further back because the incoming air has already absorbed heat from the preceding cells. Notably, the four cells at positions (2–4), (3–4), (2–5), and (3–5) receive almost no cooling effect from the airflow as they are located deep in the center of the battery pack and far from the air inlet. This observation aligns perfectly with the results reported in [13] demonstrating that the CFD simulations in this study are indeed reliable. Additionally, the cells near the outlet are better cooled than those in the center because the airflow velocity swirls and accelerates when encountering the small outlet, as shown in Fig. 5. This increases the cooling capacity of the airflow for the cells in the last column. The temperature data for each battery cell in the module is presented in Table 4.

As shown in Fig. 4, the 1 inlet – 1 outlet battery module is not effective in terms of cooling performance. Specifically, Table 4 indicates that the maximum temperature difference ΔT_{max} between the battery cells in the module is 55.76 K corresponding to 2 battery cells (2–4) and (3–1) and the temperature T_{max} of the hottest battery cell (2–4) is 361.69 K, which shows that the 1 inlet – 1 outlet module is completely unsuitable for cooling the research model. The quantitative airflow analysis for the 1 inlet – 1 outlet structure is clearly demonstrated through the velocity vectors. These vectors reveal a highly non-uniform velocity distribution: High airflow is concentrated only at the first columns of cells, while flow is severely restricted in
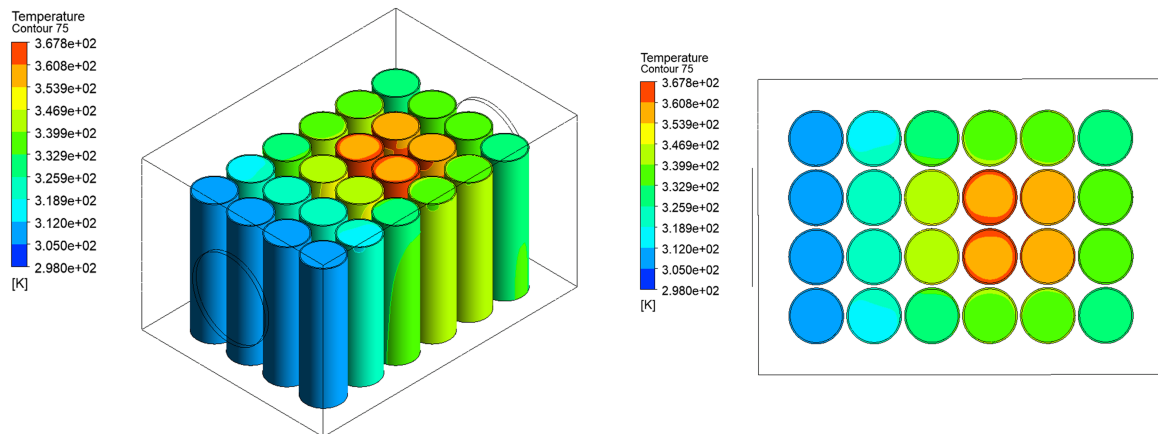

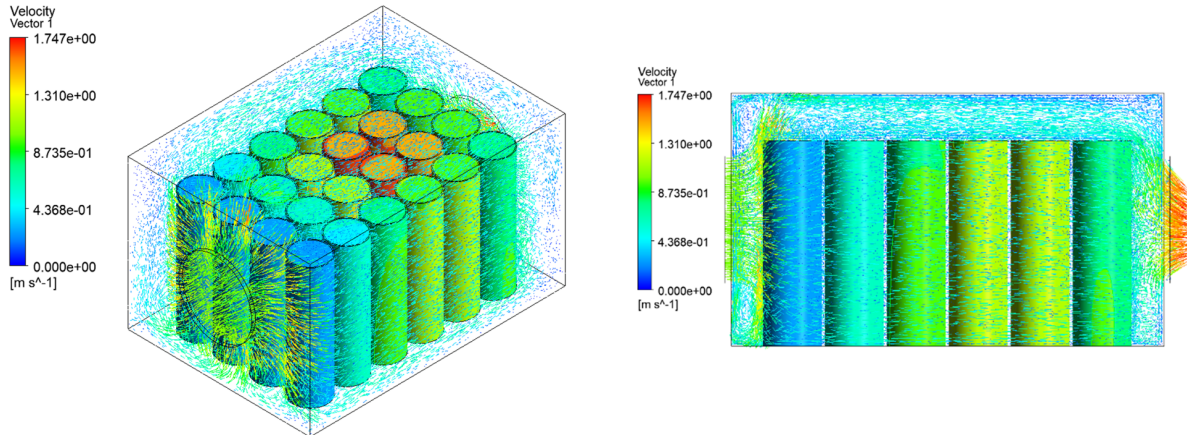Fig. 4. Thermal distribution of 1 inlet – 1 outlet structure

Fig. 5. Cool airflow in 1 inlet – 1 outlet structure

Table 4. Specific temperature of each cell in 1 inlet – 1 outlet structure

Cell	T [K]	Cell	T [K]	Cell	T [K]	Cell	T [K]
1–1	306.13	2–1	306.00	3–1	305.92	4–1	306.07
1–2	318.55	2–2	321.91	3–2	321.78	4–2	318.36
1–3	331.92	2–3	345.78	3–3	345.66	4–3	331.71
1–4	339.85	2–4	361.69	3–4	361.67	4–4	339.86
1–5	340.01	2–5	359.67	3–5	359.76	4–5	340.14
1–6	330.10	2–6	337.62	3–6	337.42	4–6	330.18

the central region, creating stagnant zones. The maximum local velocity observed within this specific model is $1.747 \, \text{m s}^{-1}$. This poor circulation is the primary cause of the extremely low thermal performance, quantified by a maximum temperature $T_{\max}$ of 361.69 K at cell (2–4) and a maximum temperature difference $\Delta T_{\max}$ reaching 55.76 K between cells (2–4) and (3–1). This outcome confirms that the 1 inlet – 1 outlet model is entirely unsuitable for meeting the ideal operating conditions. The research will continue with the 1 inlet – 2 outlets model to find a more optimal model.

B) 1 inlet – 2 outlets model
Similar to the 1 inlet – 1 outlet model, Fig. 6 shows that the 1 inlet (A) – 2 outlets (C, D) arrangement still provides the best cooling performance for the cells in the first columns. However, the cooling efficiency gradually decreases for the cells farther from the inlet as the airflow heats up from absorbing heat from the leading cells. Nevertheless, the temperatures of the four cells (2–4), (3–4), (2–5), and (3–5), which were considered critical in the 1 inlet – 1 outlet model, have been improved thanks to the additional outlet located on face D, allowing the hot air in the center of the battery pack to be effectively released, as shown in Fig. 7. The temperature of battery cells in the 1 inlet – 2 outlets model are presented in Table 5.

From Table 5, it can be seen that the 1 inlet – 2 outlets model behaves much better than the 1 inlet – 1 outlet model in reducing the maximum temperature $T_{\max}$ of the battery cell in the module to 334.75 K in cell (3–5), a decrease of 7 % compared to the original model. The decrease in $T_{\max}$ is attributed to enhanced airflow penetration into the core region, reduction of recirculating flow patterns, and a higher local convective heat transfer coefficient. The multi-vent configuration increases velocity uniformity and eliminates stagnant zones, allowing continuous removal
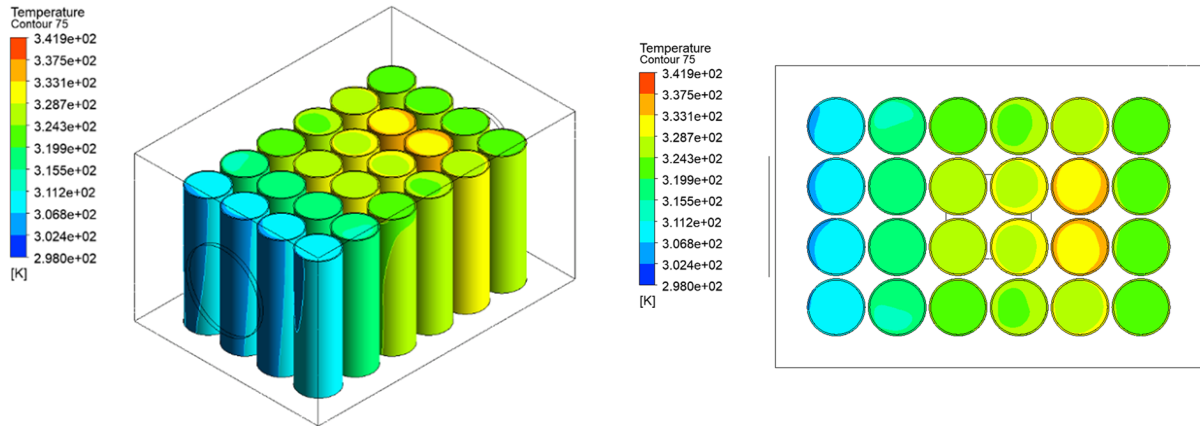
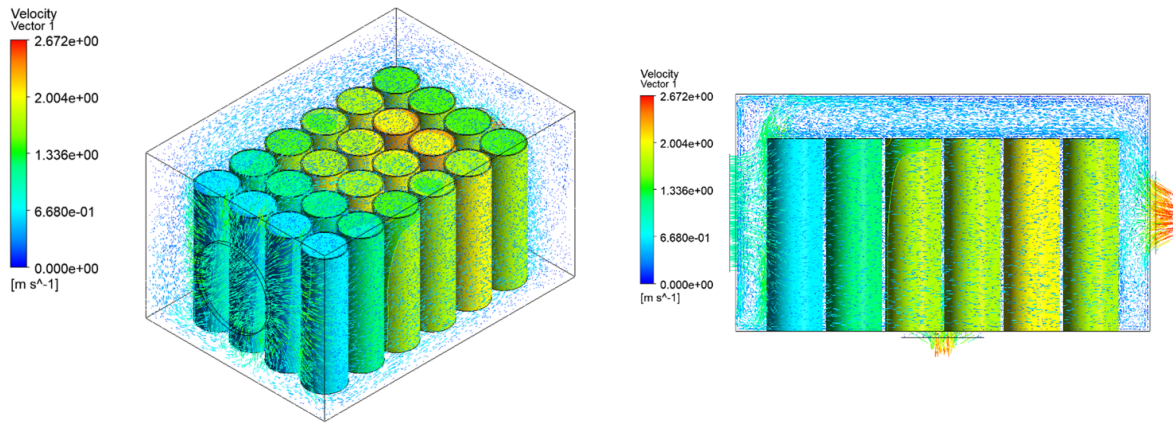Fig. 6. Thermal distribution of 1 inlet – 2 outlets structure

Fig. 7. Cool airflow in 1 inlet – 2 outlets structure

of heat from the middle battery cells. The temperature difference $\Delta T_{\max}$ is 29.31 K between cells (3–5) and (2–1), a decrease by 47 % compared to the original model. With this result, the battery module still cannot operate in the most suitable conditions, so the 1 inlet – 3 outlets model will continue to be studied in the next section.

C) 1 inlet – 3 outlets model

Based on the evaluation results from the 1 inlet – 2 outlets model, it is evident that placing a vent on side D significantly improves cooling efficiency for the cells located at the center of the battery pack. Building on this, the 1 inlet – 3 outlets model further develops the design by adding an additional vent on side B. This results in a 1 inlet model on side A and 3 outlets on

Table 5. Specific temperature of each cell in 1 inlet – 2 outlets structure

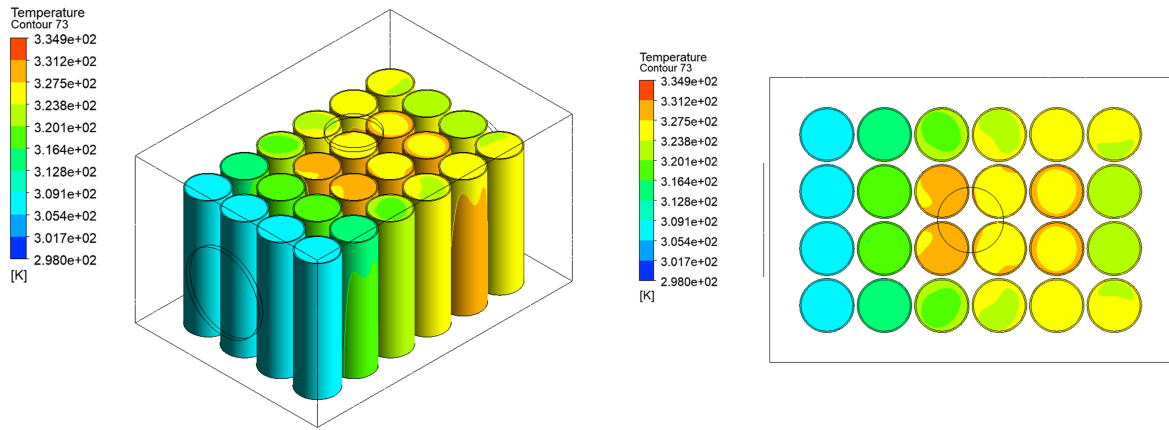| Cell	T [K]	Cell	T [K]	Cell	T [K]	Cell	T [K]
1–1	305.91	2–1	305.44	3–1	305.49	4–1	305.96
1–2	316.25	2–2	317.76	3–2	317.75	4–2	316.24
1–3	323.22	2–3	327.54	3–3	327.62	4–3	323.16
1–4	325.49	2–4	329.89	3–4	330.04	4–4	325.64
1–5	328.62	2–5	334.66	3–5	334.75	4–5	328.79
1–6	323.71	2–6	324.39	3–6	324.30	4–6	323.85

Fig. 8. Thermal distribution of 1 inlet – 3 outlets structure

sides B, C, and D, respectively. Fig. 8 shows the temperature distribution of the battery pack, which no longer exhibits the large temperature differences observed in the 1 inlet – 1 outlet model, especially for the central cells such as (2–3), (2–4), (2–5), (3–3), (3–4), and (3–5), due to the vents placed on sides B and D. The vortex strength is quantified using the velocity vector field shown in the vertical and horizontal sections in Fig. 9. This arrangement creates increased airflow vortices on top of the cells, which greatly benefits the cooling of the central cells. The columns of cells closest to the inlet continue to receive the best cooling, while the cooling efficiency gradually decreases toward the cells farther downstream. The specific temperatures of each battery cell in the 1 inlet – 3 outlets model are presented in Table 6.

Table 6 shows that the temperatures of all battery cells in the module gradually decrease and the temperature differences are not as large as before, with the maximum temperature difference $\Delta T_{\max}$ between cells (2–5) and (3–1) being 27.24 K and the highest temperature $T_{\max}$ reached by a cell in the module being 332.55 K at cell (2–5). Correspondingly, the maximum temperature and the largest temperature difference have decreased by 8 % and 51 %, respectively, compared to the first model.

From the study of the cooling efficiency of the 1 inlet – N outlet(s) models for the proposed battery module, we observe that establishing a cooling airflow from only one inlet can be effective mainly for the first few columns of cells where the air is still cool and has not been heated. As the airflow progresses toward the subsequent columns, the cooling effect diminishes because
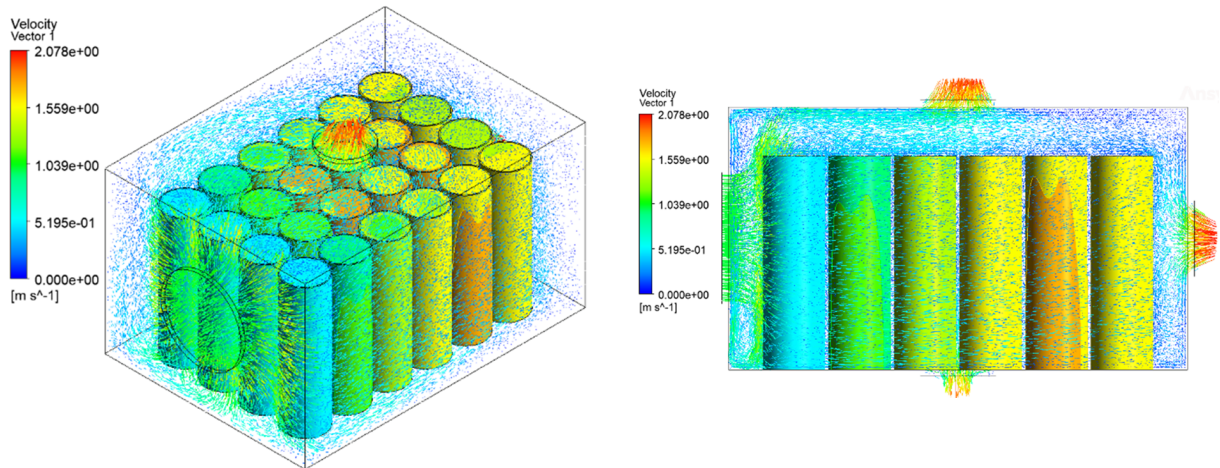

Fig. 9. Cool airflow in 1 inlet – 3 outlets structure

Table 6. Specific temperature of each cell in 1 inlet – 3 outlets structure

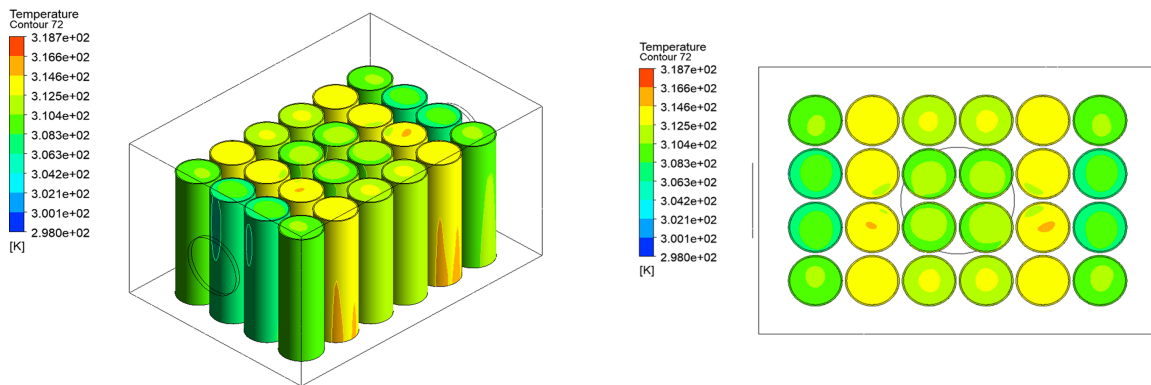| Cell	T [K]	Cell	T [K]	Cell	T [K]	Cell	T [K]
1–1	305.92	2–1	305.43	3–1	305.32	4–1	305.91
1–2	310.73	2–2	317.41	3–2	317.38	4–2	315.48
1–3	321.93	2–3	328.59	3–3	328.63	4–3	321.94
1–4	325.24	2–4	329.85	3–4	330.00	4–4	325.41
1–5	328.53	2–5	332.55	3–5	332.55	4–5	328.63
1–6	325.64	2–6	325.35	3–6	325.38	4–6	325.74

Fig. 10. Thermal distribution of 2 inlets – 1 outlet structure

the air absorbs heat from the preceding cells. Therefore, the cooling performance is very poor for the cells located at the center, where the air circulation is limited. Adding ventilation holes on faces B and D improved the cooling performance for the center cells; however, the obtained results show that the 1 inlet – N outlet(s) model still does not meet the objectives of this study. Hence, the next research focus will be on the 2 inlet – N outlet(s) model.

3.2. Thermal performance of the 2 inlets – N outlet(s) configuration

A) 2 inlets – 1 outlet model

From the simulation results of the 1 inlet – N outlet(s) model, the cooling inefficiency of the rear columns of battery cells is evident. The 2 inlets – 1 outlet model is designed with one inlet on face A and an additional inlet on face C, while the outlet is located on face D. Fig. 10 confirms the previous conclusion regarding the 1 inlet – N outlet(s) model. Adding an inlet hole on face C improves the cooling of the cells in the rear columns, and the cells in the center are also cooled effectively thanks to the ventilation hole on face D. The temperature gradient color scale shows that the temperature difference between cells has been significantly reduced. Specifically, the temperature of each battery cell is presented in Table 7.

The optimized 2 inlets – 1 outlet configuration reduces the maximum cell temperature from 361.69 to 312.62 K, corresponding to a reduction of 49.07 K (approx. 14% reduction compared to the original model), and the maximum temperature difference $\Delta T_{\max}$ is 6.74 K between cells (2–6) and (4–5) corresponding to a reduction of 88 % compared to the original model, as shown in Table 7. According to these results, the module is within the upper limit of suitable conditions for stable operation. To find an even more efficient model, the study will continue with a deeper investigation into the 2 inlets – 2 outlets model.
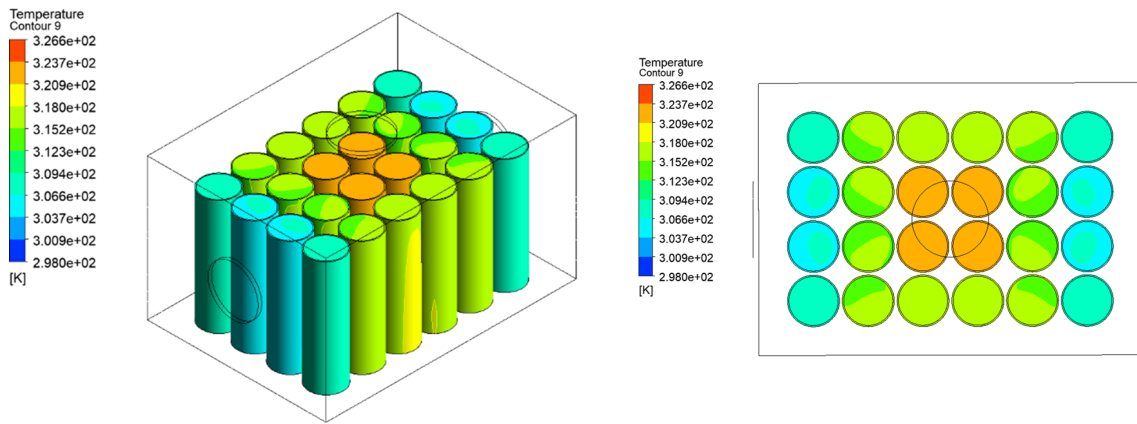
Fig. 11. Thermal distribution of 2 inlets – 2 outlets structure

B) 2 inlets – 2 outlets model

To further improve the cooling performance for centrally located cells, similar to the method studied in Section 3.1, CFD-based pre-screening confirmed that the hole locations on sides B and D minimize recirculation and improve flow uniformity, adding more vents at the center of sides B and D of the battery pack can significantly release the hot air accumulated in the middle of the battery pack, thus enhancing the cooling efficiency. Therefore, the 2 inlets – 2 outlets model, developed from the 2 inlets – 1 outlet model, adds an additional vent at the center of side B. The outlet on side B is placed along the geometric centerline to balance the flow resistance from both inlets. Its diameter is chosen to match the inlet vents so that the total vent area remains constant. However, Fig. 11 shows an undesirable result.

While this model effectively cools the cells at both ends, the temperature of the cells in the center does not improve; in fact, it is even worse compared to the 2 inlets – 1 outlet model described above. This phenomenon needs to be explained through the comparison of airflow patterns inside the module, as shown in Figs. 12 and 13. From Figs. 12 and 13, it is easy to observe that the maximum velocity at the outlet of the 2 inlets – 1 outlet model is $8.37\,\mathrm{m\,s^{-1}}$, which is significantly higher than the $3.81\,\mathrm{m\,s^{-1}}$ observed in the 2 inlets – 2 outlets model. This difference is understandable because the incoming airflow in the 2 inlets – 1 outlet model is divided between two outlets on faces B and D, whereas in the 2 inlets – 1 outlet model there is only one outlet on face D. Additionally, the airflow entering from the two inlets in the 2 inlets – 1 outlet model converges in the gap between the top of the battery cells and the module casing, then redirects downward toward the outlet on face D, creating a high-velocity vortex that further cools the cells located at the center of the battery pack.

These cells already receive cooling airflow blown from both ends along the A–C axis.

Table 7. Specific temperature of each cell in 2 inlets – 1 outlet structure

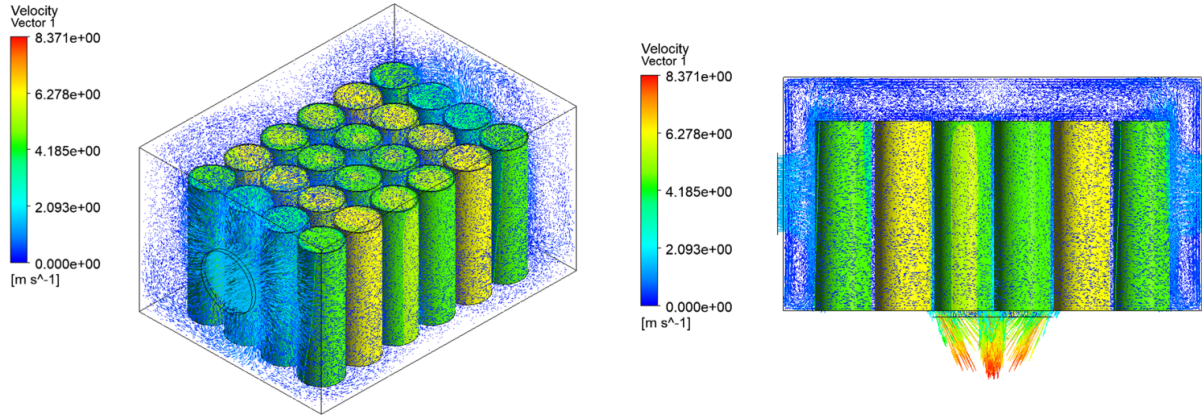| Cell	T [K]	Cell	T [K]	Cell	T [K]	Cell	T [K]
1–1	308.00	2–1	305.92	3–1	306.00	4–1	308.05
1–2	312.50	2–2	312.15	3–2	312.20	4–2	312.60
1–3	309.59	2–3	309.33	3–3	309.37	4–3	309.68
1–4	309.68	2–4	309.36	3–4	309.54	4–4	309.73
1–5	312.59	2–5	311.98	3–5	312.18	4–5	312.62
1–6	308.02	2–6	305.87	3–6	305.95	4–6	308.12

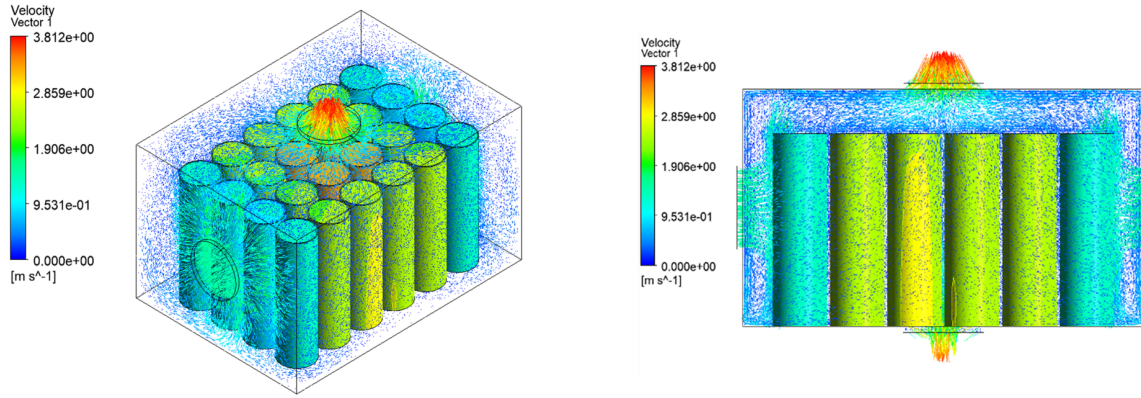Fig. 12. Cool airflow in 2 inlets – 1 outlet structure

Fig. 13. Cool airflow in 2 inlets – 2 outlets structure

Table 8. Specific temperature of each cell in 2 inlets – 2 outlets structure

Cell	T [K]	Cell	T [K]	Cell	T [K]	Cell	T [K]
1–1	307.45	2–1	305.28	3–1	305.31	4–1	307.60
1–2	315.23	2–2	314.97	3–2	314.78	4–2	315.26
1–3	317.19	2–3	321.91	3–3	321.94	4–3	317.28
1–4	317.20	2–4	321.86	3–4	321.99	4–4	317.23
1–5	315.30	2–5	314.72	3–5	314.89	4–5	315.37
1–6	307.46	2–6	305.20	3–6	305.33	4–6	307.53

In contrast, in the 2 inlets – 2 outlets model, the airflow in this gap does not converge; instead, it exits through the ventilation hole on face B, without circulating back to cool the cells. This explains why the 2 inlets – 2 outlets model cannot utilize the vortex airflow in the free space to cool the central cells as effectively as the 2 inlets – 1 outlet model does. Detailed temperature data for each cell in the 2 inlets – 2 outlets model are presented in Table 8.

As shown in Fig. 11, the temperature distribution among the cells is quite large in the 2 inlets – 2 outlets model. Table 8 clearly demonstrates this, with the highest temperature T_{max} of a cell reaching 321.99 K at cell (3–4) (an increase of 11 %) and the maximum temperature difference ΔT_{max} being 16.71 K between cells (3–4) and (2–1), a 70 % increase compared to the original model.

169

From the cooling performance analysis of the 2 inlets – N outlet(s) model, we conclude that placing two inlet openings has improved the temperature difference at the two ends of the battery module. However, the arrangement of outlet holes is also crucial. Designing multiple outlets to release hot air from the center of the battery pack is not effective. Instead, the outlet positions need to be optimized to take advantage of the vortex airflow and guide it to fully utilize the cooling capacity, as demonstrated by the 2 inlets – 1 outlet model in this study. In the following section, the 3 inlets – 1 outlet model will be examined for cooling performance compared to the 2 inlets – N outlet(s) models.

3.3. Thermal performance of the 3 inlets – 1 outlet configuration

The 3 inlets – 1 outlet model is a further development of the 2 inlets – N outlet(s) model. In this configuration, an additional inlet is added on face B, while the outlet remains on face D, enhancing the cooling capability for the cells located in the center. Fig. 14 clearly shows that the temperatures of the central cells have significantly decreased, and the cells at both ends are also effectively cooled. However, increasing the number of ventilation holes while keeping the total airflow constant results in a reduction of the diameter of each hole. This reduction significantly affects the cooling area, especially for the cells located far from the cooling axes A–C and B–D. Specifically, cells (1–2), (1–5), (4–2), and (4–5) exhibit large temperature differences compared to the cells near the air inlet openings and along the cooling air paths, as illustrated in Fig. 15. The temperature of each cell in the 3 inlets – 1 outlet model is presented in Table 9.

As shown in Fig. 15, the most difficult areas to cool within the entire module are the cells at positions (1–2), (1–5), (4–2), and (4–5), with temperatures listed in Table 9 as 316.04 K,
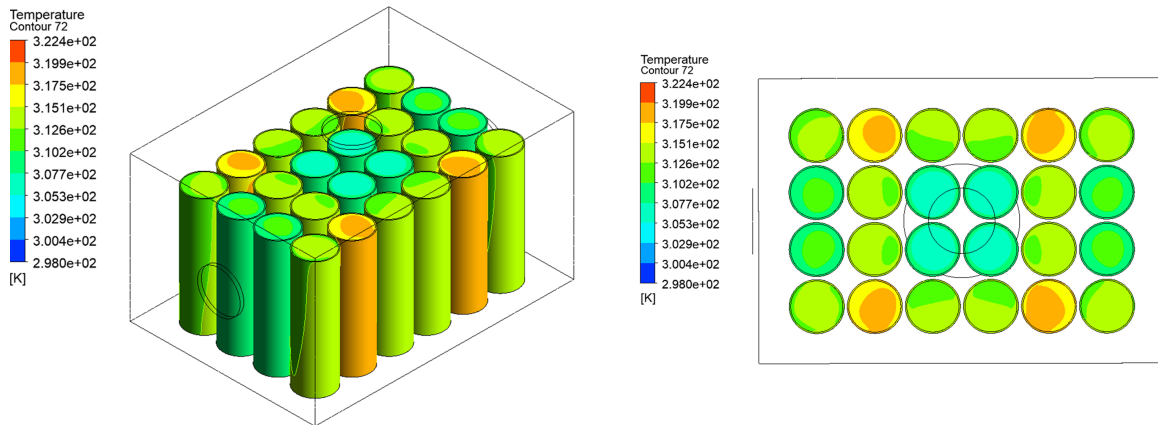

Fig. 14. Thermal distribution of 3 inlets – 1 outlet structure

Table 9. Specific temperature of each cell in 3 inlets – 1 outlet structure

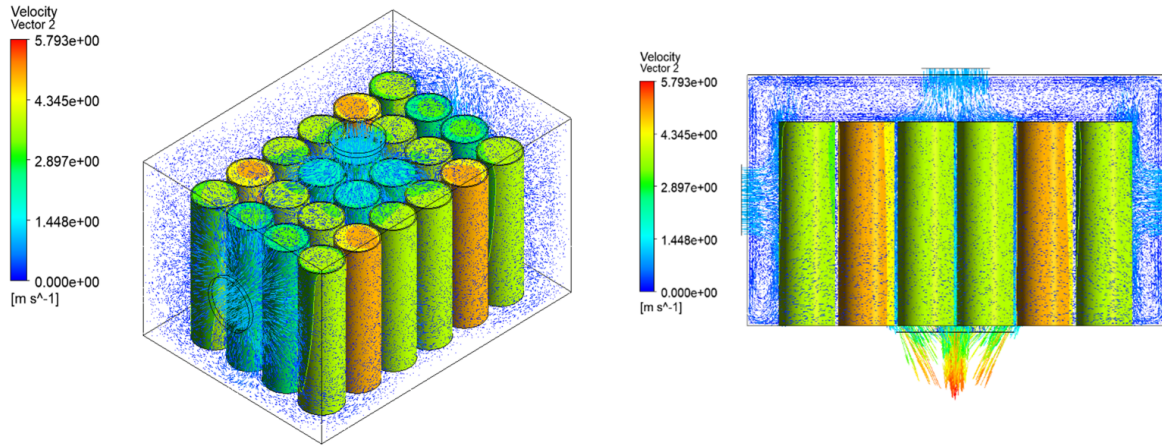| Cell	T [K]	Cell	T [K]	Cell	T [K]	Cell	T [K]
1–1	311.22	2–1	307.67	3–1	307.76	4–1	311.41
1–2	316.04	2–2	313.55	3–2	313.62	4–2	316.23
1–3	311.76	2–3	308.55	3–3	308.58	4–3	311.85
1–4	311.83	2–4	308.60	3–4	308.72	4–4	311.97
1–5	316.23	2–5	313.50	3–5	313.60	4–5	316.32
1–6	311.36	2–6	307.62	3–6	307.71	4–6	311.50

Fig. 15. Cool airflow in 3 inlets – 1 outlet structure

316.23 K, 316.23 K, and 316.32 K, respectively, representing a 13% improvement. The maximum temperature difference between cells (1–5) and (2–6) is 8.7 K, which is an 84% improvement compared to the initial model.

However, the simulation results of the 3 inlets – 1 outlet model did not meet expectations. Because the cooling effect was overly concentrated on the central cells, the airflow had to be divided into many smaller holes with reduced diameters. This led to very poor cooling for cells located far from the airflow axes or near the module casing. This issue caused a significant temperature difference within the battery module.

After studying six models with varying numbers of inlets and outlets, i.e., N inlet(s)–N outlet(s), many advantages and disadvantages of each design were identified. The best cooling performance was achieved by the 2 inlets – 1 outlet model. However, with the result of the highest cell temperature $T_{\max}$ being 312.62 K in cell (4–5) and the largest temperature difference $\Delta T_{\max}$ being 6.74 K between cells (2–6) and (4–5), it is still not suitable for the requirement of the cell temperature range in the range of 293–313 K and the temperature difference not exceeding 5 K. With such a small difference, the study will continue to improve the model by changing the velocity in the following section.

3.4. Analysis of inlet velocity effects

From the best results obtained from the six test models, the 2 inlets – 1 outlet model is doing the best in achieving the maximum temperature $T_{\max}$ and maximum temperature difference $\Delta T_{\max}$ conditions. However, it still does not meet the ideal operating conditions for the battery cells at an inlet velocity of $v = 1 \, \mathrm{m \, s^{-1}}$. In this section, the inlet velocity will be investigated at higher values ranging from 1.5 to $3 \, \mathrm{m \, s^{-1}}$ to find the optimal velocity condition for the battery module model under study. The maximum temperature and maximum temperature difference within the battery module for each tested velocity case are presented in Figs. 16 and 17.

From Figs. 16 and 17 showing the maximum temperature and maximum temperature difference of the 2 inlets – 1 outlet battery module model under increasing inlet velocity conditions, a clear trend is observed: As the velocity increases from 1 to $3 \, \mathrm{m \, s^{-1}}$, both the maximum temperature and the maximum temperature difference decrease gradually. Specifically, when the velocity increases from 1 to $3 \, \mathrm{m \, s^{-1}}$, the highest temperature of any single battery cell in the module drops from 312.62 to 304.19 K, operating entirely within the suitable temperature range of 293–313 K, even at the lowest velocity of $1 \, \mathrm{m \, s^{-1}}$. However, the temperature difference at

velocities of $1\,\mathrm{m\,s^{-1}}$ and $1.5\,\mathrm{m\,s^{-1}}$ is still above the desired threshold, with maximum temperature differences of $6.74\,\mathrm{K}$ and $5.68\,\mathrm{K}$, respectively, exceeding the target limit of $5\,\mathrm{K}$. When the velocity increases from 2 to $3\,\mathrm{m\,s^{-1}}$, this condition improves significantly, as the maximum temperature difference decreases from $4.84\,\mathrm{K}$ to $3.76\,\mathrm{K}$, fully meeting the optimal operating criteria for the battery module.

However, since the pump power is proportional to the airflow velocity, generating airflow at higher speeds will require more energy for the pump to use. The power consumption for each velocity listed in Table 10, is calculated through the following formula:

$$W_p = (p_i - p_o)\,A\,v, \tag{7}$$

where p_i, p_o are the average pressures at the inlet and outlet air streams, respectively, A is the cross-sectional area of the inlet air stream, and v is the airflow velocity.
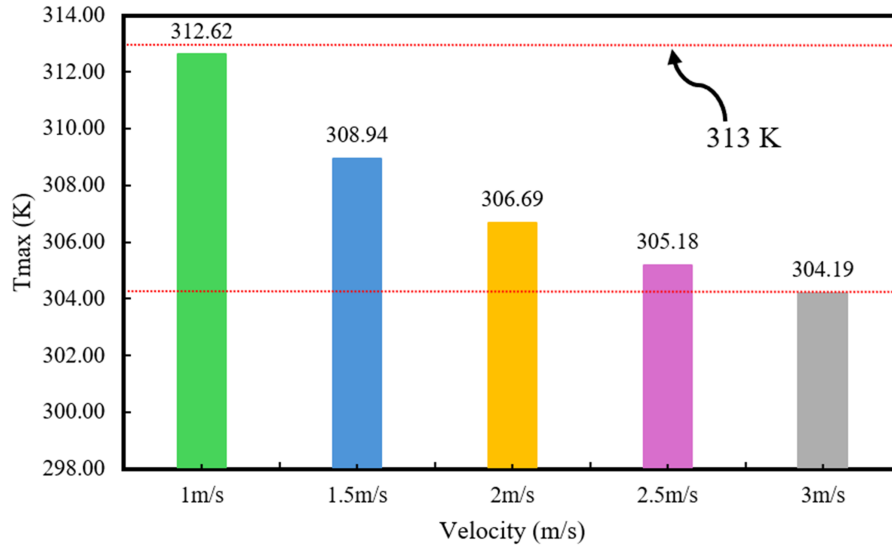

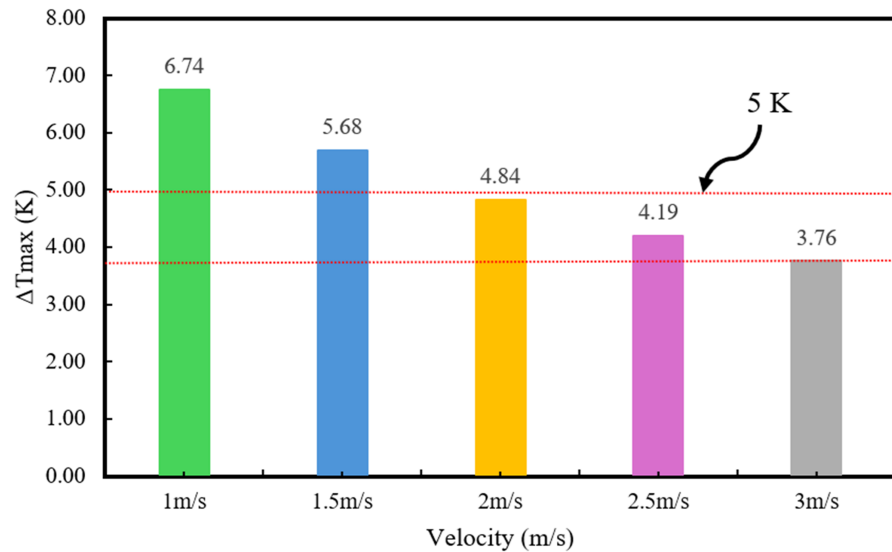Fig. 16. Maximum cell temperature in the battery module at varying inlet velocities

Fig. 17. Maximum temperature difference of a cell in the battery module at varying inlet velocities

Table 10. Power consumption at variable velocity cases

Velocity [m/s]	1	1.5	2	2.5	3
W_p [W]	0.051	0.167	0.388	0.755	1.302

As it is clear from Table 11, the pump needs to add 0.337 W to create an airflow of $2\,\mathrm{m\,s^{-1}}$ compared to the initial velocity of $1\,\mathrm{m\,s^{-1}}$, but it can be reduced by nearly 6 K with the maximum temperature and nearly 2 K with the temperature difference. Along with that, the pump power increases by 1 W but can only reduce the maximum temperature by 2.5 K and the temperature difference by 1 K. It can be seen that the higher the power, the more the cooling efficiency for the battery decreases, at the same time, more energy is wasted for the pump. This can be explained by the fact that at high velocities, the incoming cooling air has less time to interact with the battery cells, causing the uniformity of the airflow in the battery pack to decrease, thereby reducing the cooling efficiency.

Based on the study of the inlet air velocity's effect on cooling performance, the optimal velocity range for the 2 inlets – 1 outlet model, as identified in previous sections, is $2\,\mathrm{m\,s^{-1}}$. This range ensures energy savings for the cooling fan while maintaining the battery module's operation within ideal thermal conditions.

4. Conclusions

In this study, the reference model of a $4{\times}6$ battery module was investigated to improve cooling performance by dividing the airflow into multiple inlet holes to cool various critical positions more effectively. Additionally, the suitable inlet velocity for the most efficient cooling model was identified. The main conclusions of this research are summarized as follows:

1. Under the initial condition of a constant total inlet air volume, the cooling efficiency of the battery module can be improved by distributing the airflow to hard-to-cool areas such as the rear and central cells. However, cooling efficiency also depends on the placement of outlet holes to optimize the airflow direction, temperature and velocity. Excessive division of airflow into many inlets can reduce cooling performance for cells located far from the main cooling airflow paths.

2. Optimizing the size, number and position of inlet and outlet holes significantly enhances the cooling efficiency of the battery module. The case studies in this paper on the optimization of the vent structure have shown that the 2 inlets – 1 outlet model produces the best cooling effect with the highest cell temperature ($T_{\max}$) of 312.62 K at cell (4–5) and the maximum temperature difference ($\Delta T_{\max}$) of 6.74 K between cells (2–6) and (4–5).

3. The analysis of inlet velocity variations identified an optimal velocity for the 2 inlets – 1 outlet model. The results demonstrate that velocities above $2\,\mathrm{m\,s^{-1}}$ enable the battery module to maintain stable operation with $T_{\max}$ below 306.69 K (improved by 15 %) and $\Delta T_{\max}$ below 4.85 K (improved by 91 %) compared to the initial model, without consuming excessive energy for forced-air cooling fans. The proposed 2 inlet – 1 outlet concept modifies only the battery housing and does not interfere with the commercial Panasonic 18650 cell structure or safety standard. The ventilation holes can be integrated using conventional stamping processes during the module manufacturing stage.

References

[1] Abas, N., Kalair, A., Khan, N., Review of fossil fuels and future energy technologies, Futures 69 (2015) 31–49. https://doi.org/10.1016/j.futures.2015.03.003

[2] Akbarzadeh, M., Kalogiannis, T., Jaguemont, J., He, J., Jin, L., Berecibar, M., Van Mierlo, J., Thermal modeling of a high-energy prismatic lithium-ion battery cell and module based on a new thermal characterization methodology, Journal of Energy Storage 32 (2020) No. 101707. https://doi.org/10.1016/j.est.2020.101707

[3] Aneke, M., Wang, M., Energy storage technologies and real life applications – A state of the art review, Applied Energy 179 (2016) 350–377. https://doi.org/10.1016/j.apenergy.2016.06.097

[4] Becker, T. A., Tenderich, B., Sidhu, I., Electric vehicles in the United States: A new model with forecasts to 2030, Center for Entrepreneurship and Technology, University of California, Berkeley, 2009, pp. 1–32.

[5] Chen, K., Chen, Y., Li, Z., Yuan, F., Wang, S., Design of the cell spacings of battery pack in parallel air-cooled battery thermal management system, International Journal of Heat and Mass Transfer 127 (2018) 393–401. https://doi.org/10.1016/j.ijheatmasstransfer.2018.06.131

[6] Ellabban, O., Abu-Rub, H., Blaabjerg, F., Renewable energy resources: Current status, future prospects and their enabling technology, Renewable and Sustainable Energy Reviews 39 (2014) 748–764. https://doi.org/10.1016/j.rser.2014.07.113

[7] Frey, H. C., Trends in onroad transportation energy and emissions, Journal of the Air Waste Management Association 68 (6) (2018) 514–563. https://doi.org/10.1080/10962247.2018.1454357

[8] Hanif, M. A., Nadeem, F., Tariq, R., Rashid, U., Renewable and alternative energy resources, Academic Press, 2022. https://doi.org/10.1016/C2018-0-03161-8

[9] He, H., Sun, F., Wang, Z., Lin, C., Zhang, C., Xiong, R., Deng, J., Zhu, X., Xie, P., Zhang, S., Wei, Z., Cao, W., Zhai, L., China's battery electric vehicles lead the world: Achievements in technology system architecture and technological breakthroughs, Green Energy and Intelligent Transportation 1 (1) (2022) No. 100020. https://doi.org/10.1016/j.geits.2022.100020

[10] Hémery, C. V., Pra, F., Robin, J.-F., Marty, P., Experimental performances of a battery thermal management system using a phase change material, Journal of Power Sources 270 (2014) 349–358. https://doi.org/10.1016/j.jpowsour.2014.07.147

[11] Huo, J., Peng, C., Depletion of natural resources and environmental quality: Prospects of energy use, energy imports, and economic growth hindrances, Resources Policy 86 (2023) No. 104049. https://doi.org/10.1016/j.resourpol.2023.104049

[12] Jiaqiang, E., Yue, M., Chen, J., Zhu, H., Deng, Y., Zhu, Y., Deng, Y., Zhu, Y., Zhang, F., Wen, M., Zhang, B., Kang, S., Effects of the different air cooling strategies on cooling performance of a lithium-ion battery module with baffle, Applied Thermal Engineering 144 (2018) 231–238. https://doi.org/10.1016/j.applthermaleng.2018.08.064

[13] Koorata, P. K., Chandrasekaran, N., Numerical investigation of cooling performance of a novel air-cooled thermal management system for cylindrical Li-ion battery module, Applied Thermal Engineering 193 (2021) No. 116961. https://doi.org/10.1016/j.applthermaleng.2021.116961

[14] Li, X., He, F., Ma, L., Thermal management of cylindrical batteries investigated using wind tunnel testing and computational fluid dynamics simulation, Journal of Power Sources 238 (2013) 395–402. https://doi.org/10.1016/j.jpowsour.2013.04.073

[15] Li, W., Xie, Y., Yang, R., Fan, Y., Zhang, K., Panchal, S., Zhang, Y., A holistic electrothermal profiles online sensing method with sparse sensor system in large-format battery pack, IEEE Transactions on Industrial Electronics 72 (10) (2025) 10 257–10 266. https://doi.org/10.1109/TIE.2025.3555004

[16] Ling, Z., Wang, F., Fang, X., Gao, X., Zhang, Z., A hybrid thermal management system for lithium ion batteries combining phase change materials with forced-air cooling, Applied Energy 148 (2015) 403–409. https://doi.org/10.1016/j.apenergy.2015.03.080

[17] Liu, H., Wei, Z., He, W., Zhao, J., Thermal issues about Li-ion batteries and recent progress in battery thermal management systems: A review, Energy Conversion and Management 150 (2017) 304–330. https://doi.org/10.1016/j.enconman.2017.08.016

[18] Lyu, C., Song, Y., Wang, L., Ge, Y., Xiong, R., Lan, T., A new structure optimization method for forced air-cooling system based on the simplified multi-physics model, Applied Thermal Engineering 198 (2021) No. 117455. https://doi.org/10.1016/j.applthermaleng.2021.117455

[19] Luo, J., Zou, D., Wang, Y., Wang, S., Huang, L., Battery thermal management systems (BTMs) based on phase change material (PCM): A comprehensive review, Chemical Engineering Journal 430 (2022) No. 132741. https://doi.org/10.1016/j.cej.2021.132741

[20] Madani, S. S., Shabeer, Y., Fowler, M., Panchal, S., Chaoui, H., Mekhilef, S., Dou, S. X., See, K., Artificial intelligence and digital twin technologies for intelligent lithium-ion battery management systems, Batteries 11 (8) (2025) No. 298. https://doi.org/10.3390/batteries11080298

[21] Mahlia, T. M. I., Saktisahdan, T. J., Jannifar, A., Hasan, M. H., Matseelar, H. S. C., A review of available methods and development on energy storage; technology update, Renewable and Sustainable Energy Reviews 33 (2014) 532–545. https://doi.org/10.1016/j.rser.2014.01.068

[22] Merritt, H., Barragán-Ocaña, A., The impact of market factors on the development of eco-friendly energy technologies: The case of bioethanol, Clean Technologies and Environmental Policy 25 (2023) 313–321. https://doi.org/10.1007/s10098-021-02225-6

[23] Nzereogu, P. U., Omah, A. D., Ezema, F. I., Iwuoha, E. I., Nwanya, A. C., Anode materials for lithium-ion batteries: A review, Applied Surface Science Advances 9 (2022) No. 100233. https://doi.org/10.1016/j.apsadv.2022.100233

[24] Panchal, S., Khasow, R., Dincer, I., Agelin-Chaab, M., Fraser, R., Fowler, M., Numerical modeling and experimental investigation of a prismatic battery subjected to water cooling, Numerical Heat Transfer, Part A: Applications 71 (6) (2017) 626–637. https://doi.org/10.1080/10407782.2016.1277938

[25] Pham, M., Tuan, D. V., Kien, N. T., Hung, C. D., Long, L. D., Evaluation of the effectiveness of cooling channel parameters on thermal performance for electric vehicles using cylindrical lithium-ion batteries, Journal of Physics: Conference Series 2 968 (1) (2025) No. 012013. https://doi.org/10.1088/1742-6596/2968/1/012013

[26] Rao, Z., Qian, Z., Kuang, Y., Li, Y., Thermal performance of liquid cooling based thermal management system for cylindrical lithium-ion battery module, Applied Thermal Engineering 123 (2017) 1 514–1 522. https://doi.org/10.1016/j.applthermaleng.2017.06.059

[27] Sarvestani, A. B., Vakilzadeh, A. H., Javaherdeh, K., Kamali, R., Panchal, S., 3D numerical study of a novel fan-shaped heat sink with triangular cavities and nano-enhanced PCMs, Applied Thermal Engineering 280 (4) (2025) No. 128408. https://doi.org/10.1016/j.applthermaleng.2025.128408

[28] Saw, L. H., Ye, Y., Tay, A. A., Chong, W. T., Kuan, S. H., Yew, M. C., Computational fluid dynamic and thermal analysis of Lithium-ion battery pack with air cooling, Applied Energy 177 (2016) 783–792. https://doi.org/10.1016/j.apenergy.2016.05.122

[29] Saw, L. H., Tay, A. A. O., Zhang, L. W., Thermal management of lithium-ion battery pack with liquid cooling, Proceedings of the 31st Thermal Measurement, Modeling & Management Symposium (SEMI-THERM 2015), San Jose, USA, 2015. https://doi.org/10.1109/SEMI-THERM.2015.7100176

[30] Shahid, S., Agelin-Chaab, M., Development and analysis of a technique to improve air-cooling and temperature uniformity in a battery pack for cylindrical batteries, Thermal Science and Engineering Progress 5 (2018) 351–363. https://doi.org/10.1016/j.tsep.2018.01.003

[31] Shamseddine, I., Pennec, F., Biwole, P., Fardoun, F., Supercooling of phase change materials: A review, Renewable and Sustainable Energy Reviews 158 (2022) No. 112172. https://doi.org/10.1016/j.rser.2022.112172

[32] Tian, Y., Liu, X., Zhang, L., Luo, Q., Xu, Q., Yao, H., Yang, F., Wang, J., Dang, C., Xuan, Y., Prediction of thermophysical properties of chlorine eutectic salts via artificial neural network combined with polar bear optimization, Journal of Energy Storage 55 (2022) No. 105658. https://doi.org/10.1016/j.est.2022.105658

[33] Turaka, S., Obulu, P., Reddy, K. V. K., Computational fluid dynamics and thermal analysis of a lithium-ion battery with different cooling systems for electric vehicles, IOP Conference Series: Materials Science and Engineering 1136 (2021) No. 012033. https://doi.org/10.1088/1757-899X/1136/1/012033

[34] Verma, M., Phares, D., Grinbaum, I., Nanney, J., Cooling systems of large-capacity adjustable-speed drive systems, IEEE Transactions on Industry Applications 51 (1) (2014) 148–158. https://doi.org/10.1109/TIA.2014.2348073

[35] Wang, T., Tseng, K. J., Zhao, J., Wei, Z., Thermal investigation of lithium-ion battery module with different cell arrangement structures and forced air-cooling strategies, Applied Energy 134 (2014) 229–238. https://doi.org/10.1016/j.apenergy.2014.08.013

[36] Xie, J., Ge, Z., Zang, M., Wang, S., Structural optimization of lithium-ion battery pack with forced air cooling system, Applied Thermal Engineering 126 (2017) 583–593. https://doi.org/10.1016/j.applthermaleng.2017.07.143

[37] Zhang, C., Jin, X., Li, J., PTC self-heating experiments and thermal modeling of lithium-ion battery pack in electric vehicles, Energies 10 (4) (2017) No. 572. https://doi.org/10.3390/en10040572

[38] Zhang, T., Gao, C., Gao, Q., Wang, G., Liu, M. H., Guo, Y., Xiao, C., Yan, Y. Y., Status and development of electric vehicle integrated thermal management from BTM to HVAC, Applied Thermal Engineering 88 (2015) 398–409. https://doi.org/10.1016/j.applthermaleng.2015.02.001

[39] Zhang, F., Wang, P., Yi, M., Design optimization of forced air-cooled lithium-ion battery module based on multi-vents, Journal of Energy Storage 40 (2021) No. 102781. https://doi.org/10.1016/j.est.2021.102781

[40] Zhao, L., Li, W., Wang, G., Cheng, W., Chen, M., A novel thermal management system for lithium-ion battery modules combining direct liquid-cooling with forced air-cooling, Applied Thermal Engineering 232 (2023) No. 120992. https://doi.org/10.1016/j.applthermaleng.2023.120992

[41] Zhao, G., Wang, X., Negnevitsky, M., Zhang, H., A review of air-cooling battery thermal management systems for electric and hybrid electric vehicles, Journal of Power Sources 501 (2021) No. 230001. https://doi.org/10.1016/j.jpowsour.2021.230001

[42] Zhou, Y., Wang, M., Hao, H., Johnson, L., Wang, H., Hao, H., Plug-in electric vehicle market penetration and incentives: A global review, Mitigation and Adaptation Strategies for Global Change 20 (2015) 777–795. https://doi.org/10.1007/s11027-014-9611-2

[43] Zhou, H., Zhou, F., Xu, L., Kong, J., Thermal performance of cylindrical lithium-ion battery thermal management system based on air distribution pipe, International Journal of Heat and Mass Transfer 131 (2019) 984–998. https://doi.org/10.1016/j.ijheatmasstransfer.2018.11.116

[44] Živković, S., Veljković, M., Environmental impacts of the production and use of biodiesel, Environmental Science and Pollution Research 25 (2018) 191–199. https://doi.org/10.1007/s11356-017-0649-z

[45] Zuo, Q., Xie, Y., Jiaqiang, E., Zhu, X., Zhang, B., Tang, Y., Zhu, G., Wang, Z., Zhang, J., Effect of different exhaust parameters on NO conversion efficiency enhancement of a dual-carrier catalytic converter in the gasoline engine, Energy 191 (2020) No. 116521. https://doi.org/10.1016/j.energy.2019.116521